**ORIGINAL ARTICLE**

# Spectrum-sine interpolation framework for DTI processing

Yuanjun Wang[1] · Fan Jiang[1] · Yu Liu[2]

## Abstract

Diffusion tensor imaging (DTI) data interpolation is important for DTI processing, which could affect the precision and computational complexity in the process of denoising, filtering, regularization, and DTI registration and fiber tracking. In this paper, we propose a novel DTI interpolation framework named with spectrum-sine (SS) focusing on tensor orientation variation in DTI processing. Compared with the state-of-the-art DTI interpolation method using Euler angles or quaternion to represent the orientation of DTI tensors, this method does not need to convert eigenvectors into Euler angles or quaternions, but interpolates each tensor's unit eigenvector directly. The prominent merit of this tensor interpolation method lies in tensor orientation information preservation, which is different from the existing DTI tensor interpolation methods that interpolating tensor's orientation information in a scalar way. The experimental results from both synthetic and real human brain DTI data demonstrated the proposed SS interpolation scheme not only maintains the advantages of Log-Euclidean and Riemannian interpolation frameworks, such as preserving the tensor's symmetric positive definiteness and the monotonic determinant variation, but also preserve the tensor's anisotropy property which was proposed in the spectral quaternion (SQ) method.

**Keywords** Diffusion tensor MRI · Spectrum-sine interpolation · DTI mean · Riemannian manifold

## 1 Introduction

Diffusion tensor imaging (DTI), as a modality of magnetic resonance imaging (MRI), can noninvasively quantify the self-diffusion of water in vivo to obtain the structural information of human tissue for further studies, such as human white matter fiber tracking (Basser et al., 1994; [9, 10], registration [1, 11] and brain atlas construction (Hervé et al., 2011; [19, 23]). The matrix-valued data obtained by DTI, namely tensor field, is very important in the field of scientific visualization and image processing (Weickert et al., 2005). The concept of a tensor is a common physical description of anisotropic behavior, especially in solid mechanics and civil engineering, generally used in the measurement of stress, strain, inertia, permeability, and diffusion. A tensor can be defined as a $3 \times 3$ symmetric positive definite matrix [5], which can be expressed as an ellipsoid. The tensor's orientation and size are respectively represented by its eigenvectors and eigenvalue. These diffusion tensors can be used to express the fiber architectural characteristics of anisotropic fibrous tissues and organs in vivo, and they contain directional information, diffusion anisotropy, and diffusion coefficient magnitude of the microstructure information, which has important value for clinical medical analysis. However, due to the technical limitations of image acquisition, the resolution of DTI data is relatively low, such as the sparse and discontinuous myocardial part of the heart, which is misleading for clinical analysis. In addition, tensor interpolation is required to obtain information between voxels in some applications, all that makes DTI interpolation an important step in DTI processing. Diffusion tensor interpolation is a process in which tensors of known sampling voxels are used to generate tensors of unknown voxels, and then, high-resolution images are generated from low-resolution images [28].

Classical methods of DTI interpolation were completed by converting tensor information into scalar data in Euclidean space. Kindlmann et al. [12] decomposed the original

✉ Yuanjun Wang
  yjusst@126.com

✉ Yu Liu
  yliu9y@126.com

[1] Institute of Medical Imaging and Engineering, University of Shanghai for Science and Technology, Shanghai, China

[2] Department of Radiology, Shanghai Ninth People's Hospital, Shanghai JiaoTong University School of Medicine, Shanghai, China

diffusion-weighted images (DWI) into six channels of DWI scalar images, each corresponding to a pair of gradient encoding directions used during scanning acquisition, and then, values at each sampling point in the volume from these scalar images are interpolated linearly. Zhukov et al. (29) proposed reconstructing continuous tensor fields by using trilinear piecewise interpolation. Wang et al. [25] suggested a novel constrained variational principle for simultaneous smoothing and estimation of the diffusion tensor field. In the field of medical image registration, scalar interpolation methods based on the Euclidean framework have been widely used in clinical [16, 21], but it cannot guarantee the positive definiteness and invariance of tensor [13–16].

In order to overcome this problem, the concepts of affine invariant metric, logarithmic Euclidean metric, and Riemannian symmetric space metric have been introduced into a tensor field in literature [17, 18, 23], Fletcher et al., 2007; [4]. The tensor space is a manifold, which is not a vector space with the usual additive operator. Pennec et al. [17] studied partial differential equations (PDE) in the framework of affine invariants and firstly introduced the affine invariant Riemannian metric on the tensor space and treated the diffusion tensor space as a Riemannian manifold. Fletcher et al. (2007) demonstrated that the space of diffusion tensors is more naturally described as a Riemannian symmetric space, rather than a linear space, and developed a natural method for three-dimensional interpolation of diffusion tensor images based on the space formulation in this framework. Besides, the Riemannian symmetric geometry of tensors maybe allow to define an anisotropy property called geodesic anisotropy. This framework is based on geodesic interpolation and rotation interpolation proposed by Batchelor et al. [4]. In order to reduce the computational cost of the algorithm, Arsigny et al. [2] proposed a tensor interpolation method based on the logarithmic Euclidean (Log-E) metric. However, the Log-E interpolation method based on the Riemannian framework always generates a fixed determinant profile, which is not adapted to various diffusion modes in biological tissue. Therefore, Son et al. (2012) proposed a profile control method based on the non-uniform motion on a Riemannian geodesic. This method can use an arbitrary monotone profile such as linear profile, Riemannian profile, and sinusoidal profile instead of the fixed profile so that the final interpolation results can be changed with the characteristics of the diffusion model of biological tissue.

Although these interpolation methods can guarantee the monotonic variation of tensor determinant to avoid the expansion effect, the monotonicity of tensor properties is neglected. Yang et al. [27] introduced a feature-based interpolation framework for the tensor fields. In this framework, a diffusion tensor has two features in terms of its size and orientation. Through interpolating the Euler angles [6] or

quaternion [20] relevant to tensor orientation and logarithmically transformed eigenvalues, the tensor can be reconstructed from the interpolated tensor orientations and eigenvalues. This method not only preserves the symmetric positive definiteness of the tensor and the monotonic determinant variation, but also maintains the monotonicity of fractional anisotropy (FA) and mean diffusivity (MD) values. These methods achieve the goal of keeping some properties of the tensor invariable, but they ignore the anisotropy of the tensor. In order to solve this problem, Collard et al. [7] suggested a spectral quaternion (SQ) interpolation method based on quaternion, defining Hilbert anisotropic (HA) value and replacing linear quaternion interpolation weight with the weight relative to HA. The SQ method well maintains the anisotropy of interpolated tensors and improves computational efficiency. However, this method interpolates diffusion tensors by converting diffusion tensor eigenvectors into scalar quaternion data, which is not suitable for high-dimensional manifold space interpolation.

In this paper, taking into account the internal relation between tensor components, we propose a novel spectrum-sine-based interpolation framework for the diffusion tensor fields. In our, SS interpolating framework, the interpolated tensor is also represented by its eigenvalues and eigenvectors. Compared with the means about Euler angles or quaternion mentioned above [7, 27], this method does not need to convert eigenvectors into Euler angles or quaternions, but deals directly with DTI eigenvectors. Experimental results on synthetic and real human brain DTI data, both demonstrated that the SS interpolation scheme can not only maintain the advantages of Log-Euclidean and Riemannian interpolation such as preserving symmetric positive definiteness and the monotonic determinant variation, but can also preserve the anisotropy property as SQ method while saving more computational cost.

The rest of this paper is organized as follows. Section 2 introduces our interpolation framework, from two tensors interpolation, four tensors interpolation to multidimensional interpolation, together with a brief invariant property deduction during the SS interpolation. In Sect. 3, the evaluation indexes for DTI interpolation are briefly described. Section 4 gives comparison on experimental results with Log-E and SQ methods on both synthetic and real DTI data. Section 5 illustrates the results of our framework in different applications, such as filtering and regularization, followed by discussion and conclusion respectively in Sects. 6 and 7.

## 2 Methods

A diffusion tensor has two main features, including size and orientation. The tensor's size and orientation can be represented respectively by its three eigenvalues and

eigenvectors. Suppose there are two positive tensors $S_1$ and $S_2$ at point $t = 0$ and $t = 1$, then we try to interpolate the tensor $S(t)$ at point $t(0 < t < 1)$. Decompose $S_1, S_2$ as $S_1 = U_1\Lambda_1 U_1^T, S_2 = U_2\Lambda_2 U_2^T$, where $\Lambda_i = diag\left(\lambda_{i1}, \lambda_{i2}, \lambda_{i3}\right)$ with $\lambda_{i1} \geq \lambda_{i2} \geq \lambda_{i3} > 0$, $U_1, U_2$ are the orthogonal eigenvector matrices of $S_1, S_2$, $(i = 1, 2)$. For size feature interpolation, since the Log-E method gives a good solution, here we also choose their method [2]. Therefore, the interpolated eigenvalues of $S(t)$ can be written as

$$\begin{cases} \lambda'_{i1} = exp\left(tlog\lambda_{11} + (1-t)log\lambda_{21}\right) \\ \lambda'_{i2} = exp\left(tlog\lambda_{12} + (1-t)log\lambda_{22}\right) \\ \lambda'_{i3} = exp\left(tlog\lambda_{13} + (1-t)log\lambda_{23}\right) \end{cases} \quad (1)$$

For tensor's orientation feature interpolation, i.e., eigenvectors interpolation, we propose a new framework named with spectrum-sine, which will be described in the following subsections.

## 2.1 Interpolation of two tensors

For a one-dimensional case, suppose $v_1, v_2$ are the corresponding unit eigenvectors of tensors $S_1, S_2$, and the included angle of $v_1, v_2$ is $\theta$. Note the corresponding interpolated eigenvectors of $S(t)$ as $v(t)$ since $v_1, v_2$ are both unit vectors and $v(t)$ is also a unit vector. According to Fig. 1,

$$v(t) = \overrightarrow{OM} = \overrightarrow{OP} + \overrightarrow{PM} \quad (2)$$

Owing to the sine theorem, namely

$$\frac{1}{sin(\pi - \theta)} = \frac{b}{sin(t\theta)} = \frac{a}{sin((1-t)\theta)} \quad (3)$$

Then, $v(t)$ is given as

$$v(t) = \frac{sin((1-t)\theta)}{sin\theta}v_1 + \frac{sin(t\theta)}{sin\theta}v_2 \quad (4)$$

Extending the idea in Eq. (4) to DTI eigenvector matrices interpolation, suppose the eigenvector matrices $U_1, U_2$ can be decomposed of $U_i = \left(v_{i,1}, v_{i,2}, v_{i,3}\right), i = 1, 2$, whose columns are unit eigenvectors. According to Eq. (1), the interpolated eigenvalue matrix can be computed as

$$\Lambda(t) = exp\left((1-t)log\Lambda_1 + tlog\Lambda_2\right) \quad (5)$$

We also denote the interpolated eigenvectors matrix as

$$U(t) = \left(v_1(t), v_2(t), v_3(t)\right) \quad (6)$$

where $v_1(t), v_2(t), v_3(t)$ are the eigenvectors of the diffusion tensor to be interpolated. Using the same idea as in Eq. (4), we have,

$$\begin{cases} v_1(t) = \frac{sin(1-t)\theta_1}{sin\theta_1}v_{1,1} + \frac{sin\theta_1}{sin\theta_1}v_{2,1} \\ v_2(t) = \frac{sin(1-t)\theta_2}{sin\theta_2}v_{1,2} + \frac{sin\theta_2}{sin\theta_2}v_{2,2} \\ v_3(t) = \frac{sin(1-t)\theta_3}{sin\theta_3}v_{1,3} + \frac{sin\theta_3}{sin\theta_3}v_{2,3} \end{cases} \quad (7)$$

where $\theta_i = arccos\left(v_{1,i}, v_{2,i}\right), i = 1, 2, 3$ are the included angles of corresponding eigenvectors of $S_1$ and $S_2$. Equally, the interpolated orthogonal matrix $U(t)$ can be also summarized as,

$$\begin{aligned} U(t) &= (v_1(t), v_2(t), v_3(t)) \\ &= (\frac{sin(1-t)\theta_1}{sin\theta_1}v_{1,1} + \frac{sin\theta_1}{sin\theta_1}v_{2,1}, \frac{sin(1-t)\theta_2}{sin\theta_2}v_{1,2} + \frac{sin\theta_2}{sin\theta_2}v_{2,2}, \frac{sin(1-t)\theta_3}{sin\theta_3}v_{1,3} + \frac{sin\theta_3}{sin\theta_3}v_{2,3}) \\ &= \left(v_{1,1}, v_{1,2}, v_{1,3}\right)\begin{pmatrix} \frac{sin(1-t)\theta_1}{sin\theta_1} & 0 & 0 \\ 0 & \frac{sin(1-t)\theta_2}{sin\theta_2} & 0 \\ 0 & 0 & \frac{sin(1-t)\theta_3}{sin\theta_3} \end{pmatrix} + \left(v_{2,1}, v_{2,2}, v_{3,3}\right)\begin{pmatrix} \frac{sin\theta_1}{sin\theta_1} & 0 & 0 \\ 0 & \frac{sin\theta_2}{sin\theta_2} & 0 \\ 0 & 0 & \frac{sin\theta_3}{sin\theta_3} \end{pmatrix} \\ &= U_1 diag(\frac{sin(1-t)\theta_1}{sin\theta_1}, \frac{sin(1-t)\theta_2}{sin\theta_2}, \frac{sin(1-t)\theta_3}{sin\theta_3}) + U_1 diag(\frac{sin\theta_1}{sin\theta_1}, \frac{sin\theta_2}{sin\theta_2}, \frac{sin\theta_3}{sin\theta_3}) \end{aligned} \quad (8)$$

In the implementation, Schmidt orthogonalization strategy is required for interpolation correction, and the final interpolated diffusion tensor can be composed as $S(t) = U(t)\Lambda(t)U(t)^T$.

## 2.2 Interpolation of four tensors

In order to generalize one-dimensional interpolation to the two-dimension case, here we present the proposed interpolation strategy on four tensors. Given four positive tensors $S_1, S_2, S_3$, and $S_4$, the interpolated eigenvalue matrix of $S(t)$ can be computed similarly as

$$\Lambda(t) = exp\left(\sum_{i=1}^{4} t_i log\Lambda_i\right) \quad (9)$$

For eigenvector matrix part interpolation, we still denote the interpolated eigenvector matrix of $S(t)$ as $U(t) = \left(v_1(t), v_2(t), v_3(t)\right)$. What differs from two tensor interpolation cases, there exist several included angles between the four corresponding eigenvectors. Considering the eigenvectors of the interpolated tensor should be covered by the eigenvectors of $S_1, S_2, S_3$, and $S_4$, therefore, we define the interpolated eigenvectors as,
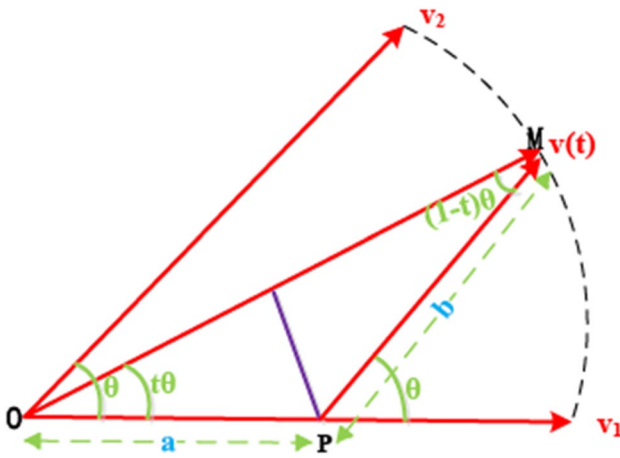
**Fig. 1** The figure of geometrical relationship between V_{1} and V_{2} vectors (Please check if figure captions are presented/captured correctly.)

$$
\begin{cases}
v_1(t) = \sum_{i=1}^{4} \frac{sin_i\theta_1}{sin\theta_1} v_{i,1} \\
v_2(t) = \sum_{i=1}^{4} \frac{sin_i\theta_2}{sin\theta_2} v_{i,2} \\
v_3(t) = \sum_{i=1}^{4} \frac{sin_i\theta_3}{sin\theta_3} v_{i,3}
\end{cases}
\tag{10}
$$

where $\theta_i = \max\limits_{m,n=1,2,3,4} \left\{ arccos\left(v_{m,i}, v_{n,i}\right) \right\}, (i = 1, 2, 3)$, $v_{m,i}$ are the $i^{th}$ eigenvector of diffusion tensor $S_m$ and $t_i$ are the corresponding weights associated with the four diffusion tensors. Therefore, the interpolated eigenvector matrix $U(t)$ can be summarized as,

$$
U(t) = \left(v_1(t), v_2(t), v_3(t)\right) = \sum_{i=1}^{4} U_i diags\left(\frac{sin_i\theta_1}{sin\theta_1}, \frac{sin_i\theta_2}{sin\theta_2}, \frac{sin_i\theta_3}{sin\theta_3}\right)
\tag{11}
$$

Finally, the tensor to be interpolated can be composed as $S(t) = U(t)\Lambda(t)U(t)^T$.

## 2.3 Multidimensional interpolation and DTI mean

Based on the definition of four tensors interpolation, it is easy to define SS interpolation in the multidimensional case. Suppose $S_1, S_2, \ldots, S_N$ is a set of diffusion tensors, which can be decomposed as $S_i = U_i\Lambda_i U_i^T, (i = 1, 2, \ldots, N)$, where $\Lambda_i = diag\left(\lambda_{i1}, \lambda_{i2}, \lambda_{i3}\right)$ and $U_i = \left(v_{i,1}, v_{i,2}, v_{i,3}\right)$. Interpolating the eigenvalue and eigenvector matrices separately, we have the interpolated eigenvalue matrix.

$\Lambda(t) = exp\left(\sum_{i=1}^{N} t_i log\Lambda_i\right)$, the eigenvector matrix

$U(t) = \sum_{i=1}^{N} U_i diag\left(\frac{sin_i\theta_1}{sin\theta_1}, \frac{sin_i\theta_2}{sin\theta_2}, \frac{sin_i\theta_3}{sin\theta_3}\right)$ with

$\theta_i = \max\limits_{m,n=1,2,\ldots,N} \left\{arccos\left(v_{m,i}, v_{n,i}\right)\right\}, (i = 1, 2, 3)$, and the final multidimensional interpolated tensor $S(t) = U(t)\Lambda(t)U(t)^T$.

Interestingly, the question about multidimensional interpolation is very similar to DTI mean in essence. As described above, the question about multidimensional interpolation is to seek a reasonable tensor based on its neighbor tensors, while the question of DTI mean is to compute a common representative tensor from a group of tensors at the same point. In other words, the interpolating weights in multidimensional interpolation are designed according to the distance from local neighbor tensors, and the weights used in computing DTI mean are estimated by minimizing the target function that measures the distance from the mean tensor to the others. Now we present the solution on DTI mean question based on the proposed SS interpolation framework.

The Fréchet mean is well known in application; for DTI mean, this definition is described as,

$$
S_{\text{mean}}\left(S_1, S_2, \ldots, S_N\right) = \underset{S}{argmin} \sum_{i=1}^{N} w_i \text{dist}^2\left(S, S_i\right)
\tag{12}
$$

where the distance measure $\text{dist}(\cdot, \cdot)$ gives the distance between two tensors, $w_i$ are the weights, and the optimized solution is the DTI mean tensor $S_{\text{mean}}$. In the affine invariant framework, the computation of the DTI mean needs a large number of use of matrix exponential, logarithm, inverse, and square root operations [17], which makes DTI processing very complex. Since the tensor space of logarithmic Euclidean metric has actually the same form as the corresponding Euclidean transformation space of the symmetric matrix, the Log-Euclidean Fréchet mean is generalized as (Moakher M, 14),

$$
S_{\text{LEmean}}\left(S_1, S_2, \ldots, S_N\right) = exp\left(\sum_{i=1}^{N} w_i log\left(S_i\right)\right)
\tag{13}
$$

The Log-Euclidean method provides a much simpler strategy for the mean tensor calculation.

The solution for DTI mean question using the proposed SS interpolation framework is consistent with that of the SQ method, in which the mean tensor is defined with two different components: mean eigenvalue and mean orientation. Given $N$ positive weights $\omega_1, \ldots, \omega_N$ that satisfy $\sum_{i=1}^{N} \omega_i = 1$, and the weighted mean of $N$ tensors $S_1, \ldots, S_N$ is defined by $S_{\text{mean}} = U_{\text{mean}}\Lambda_{\text{mean}}U_{\text{mean}}^T$, where the different components $U_{\text{mean}}$ and $\Lambda_{\text{mean}}$ are defined as follows. As shown in Eqs. (9, 11), here the weighted mean eigenvalue matrix is defined as,

$$
\Lambda_{\text{mean}} = exp\left(\sum_{i=1}^{N} \omega_i log\Lambda_i\right)
\tag{14}
$$

and the mean eigenvector matrix can be computed according to the equation

$$U_{\text{mean}} = \sum_{i=1}^{N} U_i diag\left(\frac{sin\omega_i\theta_1}{sin\theta_1}, \frac{sin\omega_i\theta_2}{sin\theta_2}, \frac{sin\omega_i\theta_3}{sin\theta_3}\right) \quad (15)$$

This is different from that of the SQ method. For mean orientation estimation, the SQ method consists in selecting the tensor with the largest mean of Hilbert anisotropy as the reference quaternion firstly, then realign the quaternion, and finally get the mean quaternion. Here the SS method performs a direct orientation interpolation, without choosing any reference tensor; therefore, the estimated DTI orientation matrix depends on all the original tensors, with no dependence on any special reference tensors.

### 2.4 Invariant properties of SS

Invariant properties are important for DTI processing, as reported in Collard et al. [7], the SQ interpolation formula is shaped invariant by scaling, congruence, and even general linear group. According to SS interpolation formulas (5, 8), for scaling invariant property, if $\alpha > 0$,

$$\begin{aligned}
&S(t;\alpha S_1;\alpha S_2)\\
&= Uexp\big((1-t)log(\alpha S_1) + tlog(\alpha S_2)\big)U^T\\
&= Uexp\big(log\alpha + (1-t)logS_1 + tlogS_2\big)U^T\\
&= \alpha Uexp\big((1-t)logS_1 + tlogS_2\big)U^T\\
&= \alpha S(t;S_1;S_2)
\end{aligned} \quad (16)$$

This shows that the SS interpolate satisfies the shape invariant property. Compared to shape invariant property, orientation invariant property is more attractive. Denote $SO(3)$ as the special orthogonal group of rotation matrices with determent equal to 1, $\forall M \in SO(3)$,

$$S(t;MS_1M^T;MS_2M^T) = S\big(t;MU_1\Lambda_1(MU_1)^2\big) \triangleq U'(t)\Lambda(t)U'(t)^T \quad (17)$$

where

$$\begin{aligned}
U'(t) = &MU_1 diag\big(\tfrac{sin(1-t)\theta_1}{sin\theta_1}, \tfrac{sin(1-t)\theta_2}{sin\theta_2}, \tfrac{sin(1-t)\theta_3}{sin\theta_3}\big) + MU_2 diag\big(\tfrac{sint\theta_1}{sin\theta_1}, \tfrac{sint\theta_2}{sin\theta_2}, \tfrac{sint\theta_3}{sin\theta_3}\big)\\
&M(U_1 diag\big(\tfrac{sin(1-t)\theta_1}{sin\theta_1}, \tfrac{sin(1-t)\theta_2}{sin\theta_2}, \tfrac{sin(1-t)\theta_3}{sin\theta_3}\big) + U_2 diag\big(\tfrac{sint\theta_1}{sin\theta_1}, \tfrac{sint\theta_2}{sin\theta_2}, \tfrac{sint\theta_3}{sin\theta_3}\big))\\
&= MU(t)
\end{aligned} \quad (18)$$

Therefore,

$$S(t;MS_1M^T;MS_2M^T) = MU(t)\Lambda(t)U(t)^T M^T = MS(t;S_1;S_2)M^T \quad (19)$$

What shows the SS interpolate formula satisfies the orientation invariant property under elementary rotation transformation. Similarly, we can deduce the scaling and rotation invariant formula,

$$S(t;\alpha MS_1M^T;\alpha MS_2M^T) = \alpha MS(t, S_1, S_2)M^T \quad (20)$$

## 3 Evaluation measures of DTI interpolation strategy

In this section, we introduce a range of measurements, which can be used to evaluate different DTI interpolation methods. A diffusion tensor can be classified by its size, shape, and orientation. We evaluate different interpolation methods on the basis of their sensitivity to the changes in these properties. For an interpolation method, the general evaluation properties are mainly divided into the following two categories: (1) DTI scalar indices evaluation and (2) DTI orientation angular difference.

### 3.1 DTI scalar indices evaluation

The easiest way to get the difference between two diffusion tensors $S_1$ and $S_2$ is to compare the absolute difference of their scalar indices (Peeters 15). These indices reduce the 6D information in a tensor to a scalar value. Several kinds of commonly used measures, including mean diffusivity (MD), fractional anisotropy (FA), relative anisotropy (RA) [3], geodesic anisotropy (GA) [8], and Hilbert anisotropy (HA) [7] are introduced in Table 1. These measures are defined by the eigenvalues and they are rotation invariant.

### 3.2 DTI orientation evaluation

The scalar indices mentioned above are related to tensor shape and size, and the orientation information of diffusion tensor is related to tensor's eigenvectors, which is important to fiber tractography. For tensor orientation evaluation, we employ the included angle of two tensors' corresponding eigenvectors [24].

$$IA = arccos\big(v_{i1} \cdot v_{i2}\big), i = 1, 2, 3. \quad (21)$$

where $v_{i1}, v_{i2}$ are the principal eigenvectors of different tensors $S_1$ and $S_2$. A smaller $IA$ value means a better orientation overlap. In practice, since the principal eigenvectors determine the direction of fiber tractography which is important in the application, therefore we compute the $IA$ measure of the principal eigenvectors only.

## 4 Experiments

In this paper, simulated diffusion tensor data and real DTI data are used to verify the proposed SS interpolation method, which is compared with the SQ and the Log-E interpolation methods. In order to fully consider the interpolated tensors,

the synthetic data constructed in this experiment include anisotropic and isotropic tensors of different sizes. Therefore, the merits and demerits of these three interpolation methods are investigated comprehensively and systematically.

## 4.1 Synthetic tensor data experiments

Firstly, the interpolation experiments of three different methods are carried out using the synthetic tensor data for the interpolation of two tensors. In order to fully observe the variation of tensor to be interpolated, the synthetic data in this experiment have the same shape in different orientations. Firstly, the orientation is determined according to the pre-defined rotation matrix $R$ of a tensor with different angles $\alpha$, and then, the size of this tensor is determined by selecting different eigenvalues. Let $S(t)$ denote a series of tensors, in which $S(0) = S_1$, $S(1) = S_2$, and the other tensors in $S(t)$ are interpolated equally between 0 and 1 with step $\Delta t = 0.125$. The orientation of $S_1$ and $S_2$ is determined according to the defined rotation matrix $R = \begin{pmatrix} cos\alpha & -sin\alpha & 0 \\ sin\alpha & cos\alpha & 0 \\ 0 & 0 & 1 \end{pmatrix}$ with different angles $\alpha_1 = 2\pi/360$, $\alpha_2 = 2\pi \times 63/360$, and the shape changes are controlled by the size of eigenvalues $\Lambda_1 = diag(10, 1, 1)$, $\Lambda_2 = diag(40, 4, 1)$.

Figure 2 shows the interpolation results of the SQ, Log-E, and SS methods between two tensors. Figure a, b, and c present the interpolated tensors of SQ, Log-E, and SS methods, and Figure d computes the evaluation indices of tensor size, shape, and orientation. According to the change of color and shape of the ellipsoid in Fig. 2, it can be seen that the interpolated tensors corresponding to $t = 0.625 : 1$ of the Log-E method tend to be isotropic, and the change on tensor's orientation of Log-E interpolation is too abrupt, while the SQ and SS interpolation methods both present a gradual interpolation process. In Figure d, from left to right, the horizontal axis represents the parameter $t$ and the

**Table 1** Scalar indices for diffusion tensors

| Scalar index | Equation |
| --- | --- |
| Mean diffusivity | $MD = (\lambda_1 + \lambda_2 + \lambda_3)/3$ |
| Fractional anisotropy | $FA = \sqrt{\dfrac{3\sum_{i=1}^{3}(\lambda_i - \bar{\lambda})^2}{2\sum_{i=1}^{3}\lambda_i^2}}$ |
| Relative anisotropy | $RA = \sqrt{\dfrac{\sum_{i=1}^{3}(\lambda_i - \bar{\lambda})^2}{3\bar{\lambda}}}$ |
| Geodesic anisotropy | $GA = \sqrt{\sum_{i=1}^{3}\left(log(\lambda_i) - log\left(\sqrt[3]{\lambda_1\lambda_2\lambda_3}\right)\right)^2}$ |
| Hilbert anisotropy | $HA = log(\lambda_{max}/\lambda_{min})$ |

longitudinal axis represents the determinant (Det), fractional anisotropic (FA), Hilbert anisotropic (HA), and the principal eigenvectors included angle (IA) respectively. From Fig. 2, we can see that for tensor determinant variation curves, the determinant curves of the three interpolation methods overlap, which shows that the determinant changes of these three methods are coincident, showing a monotone increasing trend. From the second and third figure of (d), for the variation of FA and HA, only the SQ and SS methods are monotonic. The Log-E method has a minimum value in the second figure of (d), this indicates that the Log-E method collapses for FA and HA values at some interpolated tensor, where the tensor is more like isotropic while the anisotropy is restrained.

For tensor orientation evaluation in the last figure of Fig. 2d, the difference between SQ, Log-E, and SS is obvious, while the difference between SQ and SS is hard to observe. In fact, there is a small difference between SQ and SS methods. In order to show this difference clearly, we compute the differentiation of the IA curve in Fig. 2d, which is presented in Fig. 3a. In the Log-E interpolation method, the tensor's orientation changes greatly from the first tensor to the last tensor, and both the SQ and SS methods display the tensor's orientation changes gradually. To be precise, the tensor's orientation of the SS method changes equally according to the circle arc while the orientation of the SQ method changes equally according to the circle chord, which leads to the IA index changes equally for SS, symmetrically for SQ. The precise quantitative values of mark points in Fig. 2d are presented in Fig. 3b, a small difference exists between SQ and SS.

The second synthetic tensor data experiment is to verify the effectiveness of SS for four tensors' interpolation. Using the same synthetic data generation strategy as in the above two tensors' interpolation experiment, we define four tensors $S_1$, $S_2$, $S_3$, and $S_4$ with $\alpha_1 = \frac{\pi}{3}$, $\alpha_2 = \frac{\pi}{4}$, $\alpha_3 = \frac{\pi}{2}$, $\alpha_4 = 0$, and $\Lambda_1 = diag(1, 0.95, 0.9)$, $\Lambda_2 = \Lambda_3 = \Lambda_4 = diag(2, 0.25, 0.1)$, which are placed at four corners of the rectangle region from the bottom left corner to the top left corner counterclockwise. As displayed in Fig. 4, $S_1$ is approximate to an isotropy tensor, $S_2$, $S_3$, and $S_4$ are linear shape anisotropy tensors with different orientations. The interpolation experiment is to estimate the tensors distributed on the uniform grid points within the rectangle region.

Using the proposed SS framework on four tensors' interpolation, the interpolation results are presented in Fig. 4. In the first column of Fig. 4, the top, middle, and bottom figures are the interpolation results of SS, SQ, and Log-E methods respectively. According to the shape and color changes of these ellipsoidal tensors shown in Fig. 4, the difference of interpolated tensors between SS, SQ, and Log-E method is obvious, while the interpolation performance between SS and SQ is hard to distinguish. In
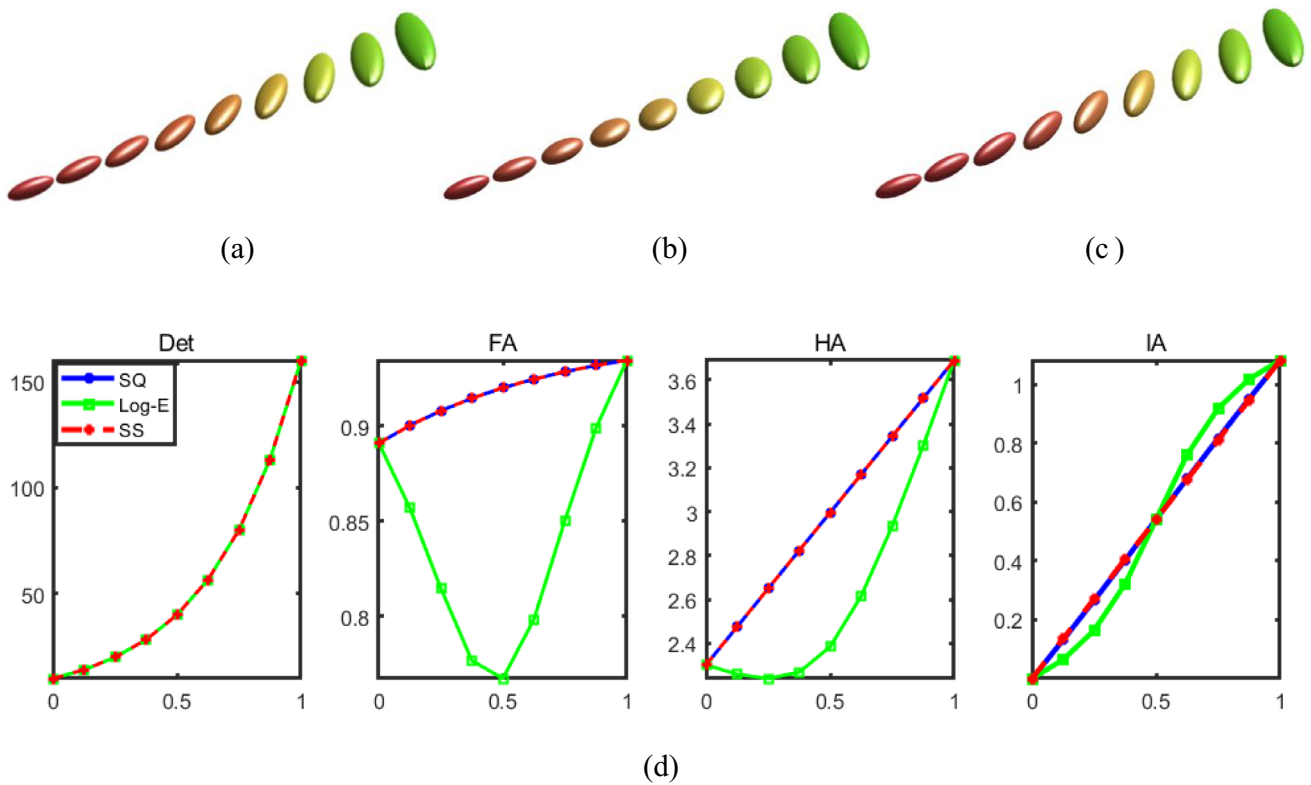
Fig. 2 Interpolation results of two tensors. Panels **a**, **b**, and **c** are the interpolation results of SQ, Log-E, and SS methods respectively. Panel **d**, from left to right, the determent index, FA and HA indices, and the IA index of the principal eigenvectors between S_1 and interpolated tensors

the second column of Fig. 4, the corresponding principal eigenvectors direction maps are displayed, and a large difference can be seen from the Log-E method, but only little difference between SS and SQ. The last column figures are the corresponding HA contour maps of SS, SQ, and Log-E. Both SS and SQ methods present a uniformly distributed contour map.

In order to further compare the difference between SS and SQ methods, we compute the weighted angles between each interpolated tensors and the four given tensors, which is

defined as $WA(i,j) = \sum_{k=1}^{4} \omega_{ij} arccos(e_k \cdot e_{ij})$, where $\omega_{ij}$ is the weight at a grid point $(i,j)$, $e_{ij}$ is the principal eigenvector of the interpolated tensor $S(i,j)$, and $e_k, k = 1, 2, 3, 4$ are the principal eigenvector of $S_k$. As expected, the weighted angle index of SS is a little smaller than that of SQ and Log-E at all the inner grid points, and the WA index is consistent with the result of two tensors' interpolation at the border interpolated grid points. The final average WA indices for the three methods are $WA_{SS} = 0.3595$, $WA_{SQ} = 0.3851$, and

Fig. 3 Detailed tensor orientation changes comparison corresponding IA index in Fig. 2d. **a** Differentiation of IA corresponding with three different methods; **b** quantitative values of mark points in Fig. 2d
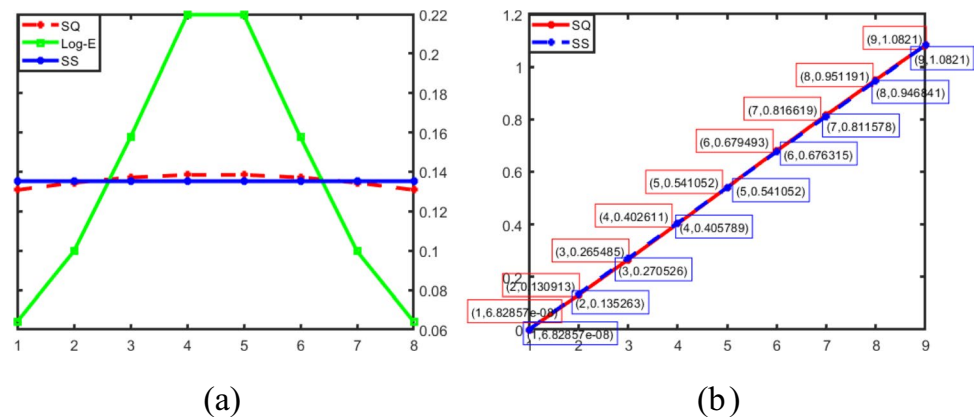
**Fig. 4** Interpolation results of four tensors. Topline: **a** interpolation results of SS method, **b** the principal eigenvectors direction map of **a**, **c** the HA contour map of a; middle line: **d** the interpolation results of SQ, **e** the principal eigenvectors direction map of **d**, **f** the HA contour map of **d**; bottom line: **g** the interpolation results of Log-E, **h** the corresponding principal eigenvectors direction map of **g**, **i** the HA contour map of **g**
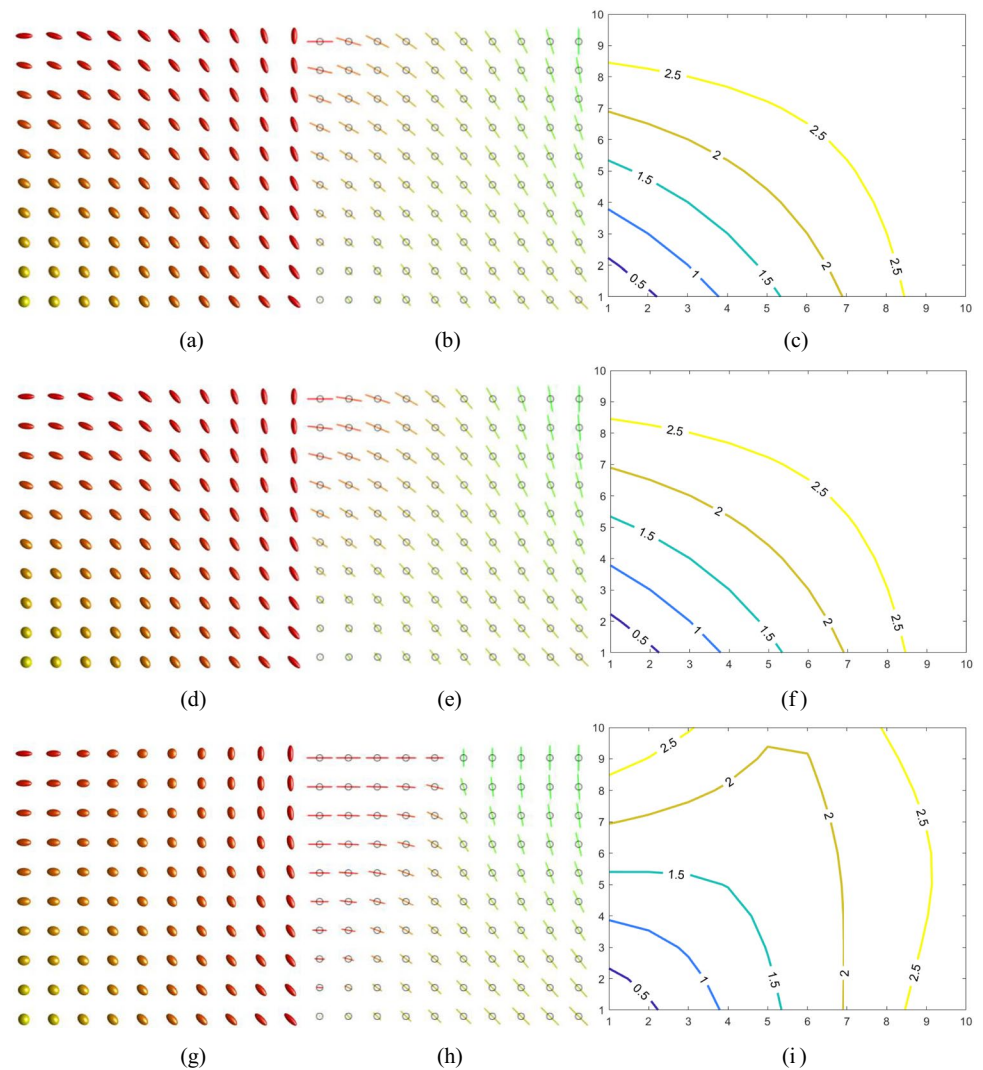


$WA_{Log-E} = 0.3989$. In order to observe the vision effect difference of both SS and SQ methods, we present the overlap principal eigenvectors direction map in the following Fig. 5. After calculating the angle between adjacent principal eigenvectors in one row, we find that the principal eigenvector direction of SS varies uniformly, while the principle direction of SQ changes a little bigger at the beginning and end points than the middle points.

### 4.2 Real DTI data experiments

In order to further verify the interpolation performance of the proposed SS framework, we now perform SS on real DTI data by comparing it with SQ and Log-E methods. In this experiment, the brain DTI data was acquired from Shanghai Ninth People's Hospital, and the matrix size is $128 \times 128 \times 60$ with a $2 \times 2 \times 2$ mm$^3$ voxel size, and the

*b*-value is 800 s mm$^{-2}$, and the scanning series is EPI. To observe the interpolation performance clearly, only a $41 \times 41$ region of interest (ROI) focusing on the corpus callosum is chosen for interpolation methods validation, which is shown in Fig. 6a. In this experiment, the DTI data is firstly downsampled to $21 \times 21$ in Fig. 6b, and then, interpolating the downsampled tensor field to original resolution with SS, SQ, and Log-E methods.

In order to display the interpolation results clearly, this study selects two small regions in Fig. 6b with black and red rectangles, where the black rectangle region focuses on anisotropy tensors interpolation while the red rectangle focuses on relative isotropy tensors interpolation. The interpolation results focusing on the black rectangle region are displayed in Fig. 7. For comparison, the original tensor image together with the SS, SQ, and Log-E interpolated images around the black rectangle are displayed. As the

**Fig. 5** The overlap of SS, SQ principal eigenvector directions. The solid line is the SS principal eigenvectors direction and the dotted line is the SQ principal eigenvectors' direction
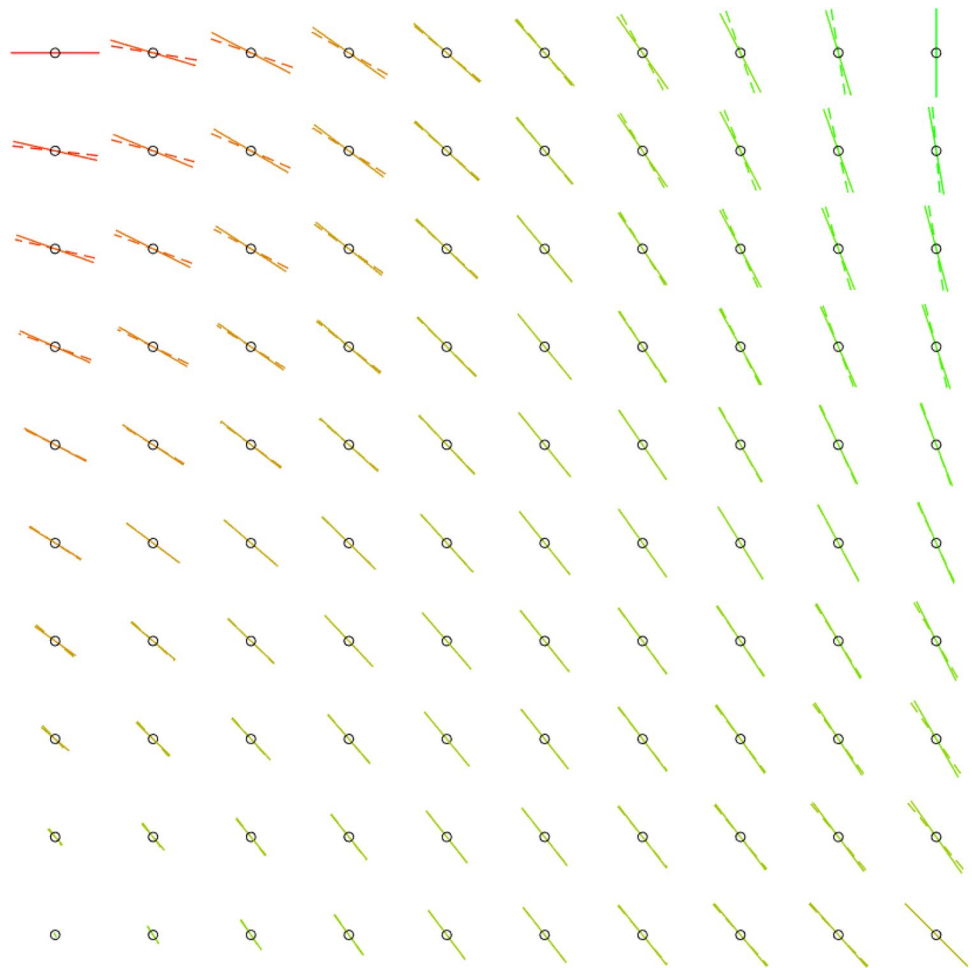


tensors' shape and orientation change slowly in real DTI data, the difference between three different methods is very small. To observe the black rectangle region carefully, it can be seen that the SS interpolation results show a better shape and orientation variation. For quantitative evaluation, the evaluation measures described in the previous section are computed in Fig. 7a–d respectively. The difference between SS, SQ, and Log-E methods and the original images are summarized in Table 2, and a small value means better interpolation performance. Since the eigenvalue interpolation strategy is the same in SS and SQ methods, the HA, FA, MD, and Det indices show the same performance, while the tensor's orientation index IA shows some difference. The IA index of the SS method is the smallest, which indicates that the SS method has the best orientation preservation ability.

The red rectangle region interpolation results are shown in Fig. 8. A very similar performance to the

black rectangle region is completed by SS, SQ, and Log-E methods, which shows that the region with much anisotropy (black rectangle region) or much isotropy (red rectangle region) has no effect on all the three interpolation methods. Quantitative indices are compared similarly and summarized in Table 3. The IA index shows some decrease in the SS method with respect to SQ and Log-E, and the other indices show no difference.

In addition, in order to observe the whole contour of the corpus callosum, according to the three methods interpolated results, we select a specific boundary area around the corpus callosum. The interpolated tensor fields of SS, SQ, and Log-E methods are presented in Fig. 9, the corresponding FA indexes are computed. From Fig. 9a to d, the boundaries of the three methods are preserved well. However, from the corresponding FA images, SS and SQ present a much better contour performance than Log-E.

**Fig. 6** Real brain DTI data experiment. **a** 41×41 corpus callosum ROI; **b** downsampling of **a**



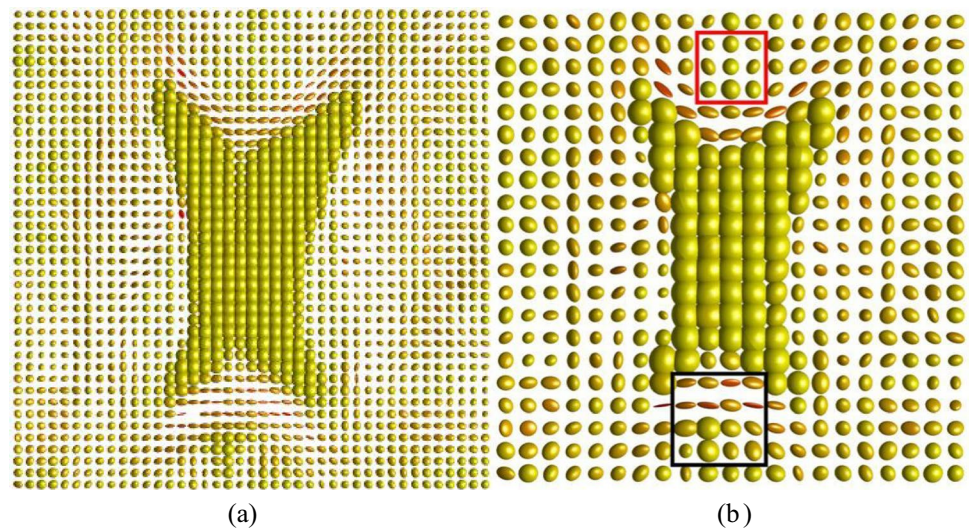(a)                                              (b)

**Fig. 7** Interpolation results focusing on the black rectangle region. **a** Original tensor image; from **b** to **d**, the results of SS, SQ, and Log-E methods respectively
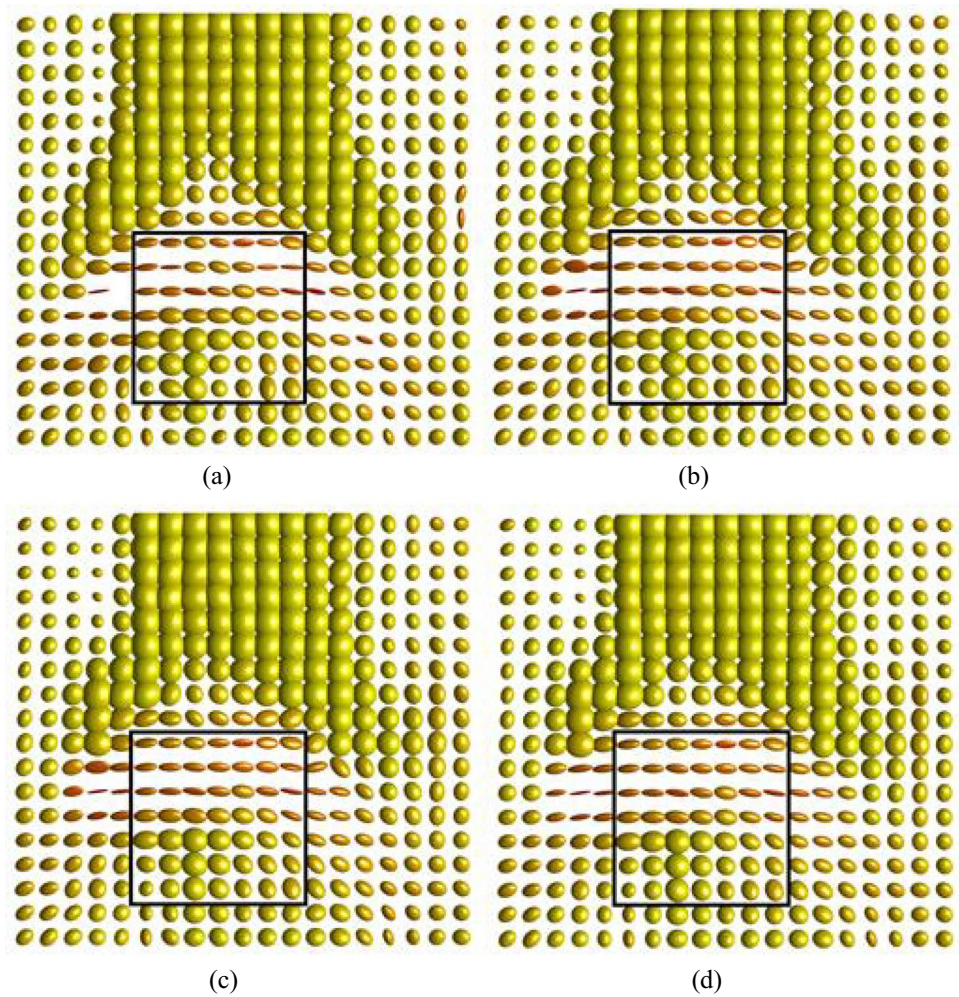


(a)                                              (b)



(c)                                              (d)

**Table 2** Error analysis of three interpolation methods in the black rectangle region

| Methods | HA | FA | MD ($10^{-8}$) | Det ($10^{-19}$) | IA |
|---|---|---|---|---|---|
| SS | 0.1372 | 0.0048 | 1.6170 | 2.6981 | 1.1314 |
| SQ | 0.1372 | 0.0048 | 1.6170 | 2.6981 | 1.1965 |
| Log-E | 0.1580 | 0.0056 | 1.6223 | 2.6981 | 1.2583 |

**Table 3** Error analysis of three interpolation methods in the red rectangle region

| Methods | HA | FA | MD ($10^{-9}$) | Det ($10^{-20}$) | IA |
|---|---|---|---|---|---|
| SS | 0.0080 | 0.0018 | 6.5874 | 4.2373 | 0.8871 |
| SQ | 0.0080 | 0.0018 | 6.5874 | 4.2373 | 0.8989 |
| Log-E | 0.0176 | 0.0044 | 6.3463 | 4.2373 | 0.9407 |

## 5 DTI processing with SS interpolation

In this section, we further develop some DTI processing methods based on the proposed SS interpolation framework, together with the multidimensional interpolation strategy and DTI mean. Filtering and regularization are basic in DTI data processing; therefore, we present these two DTI processing algorithms in the following. To be pointed out, the proposed SS framework and the definition of DTI mean can be further used in many other applications, such as DTI registration and brain template construction.

## 5.1 Gaussian filtering of DTI

The concept of DTI weighted mean based on the SS interpolation framework provides novel ideas for DTI processing, and Gaussian filtering is one of the most widely used technique. Here, we apply the weighted mean of SS interpolation to Gaussian filtering, and experimental results are shown in Fig. 10. In this experiment, the size of the Gaussian filter is $3 \times 3 \times 3$, and the Gaussian kernel parameter $\sigma = 0.5$. In Fig. 10, figure (a) is the original tensor data focusing on



**Fig. 8** Interpolation results focusing the on red rectangle region. **a** Original tensor image; from **b** to **d**, the results of SS, SQ, and Log-E methods respectively
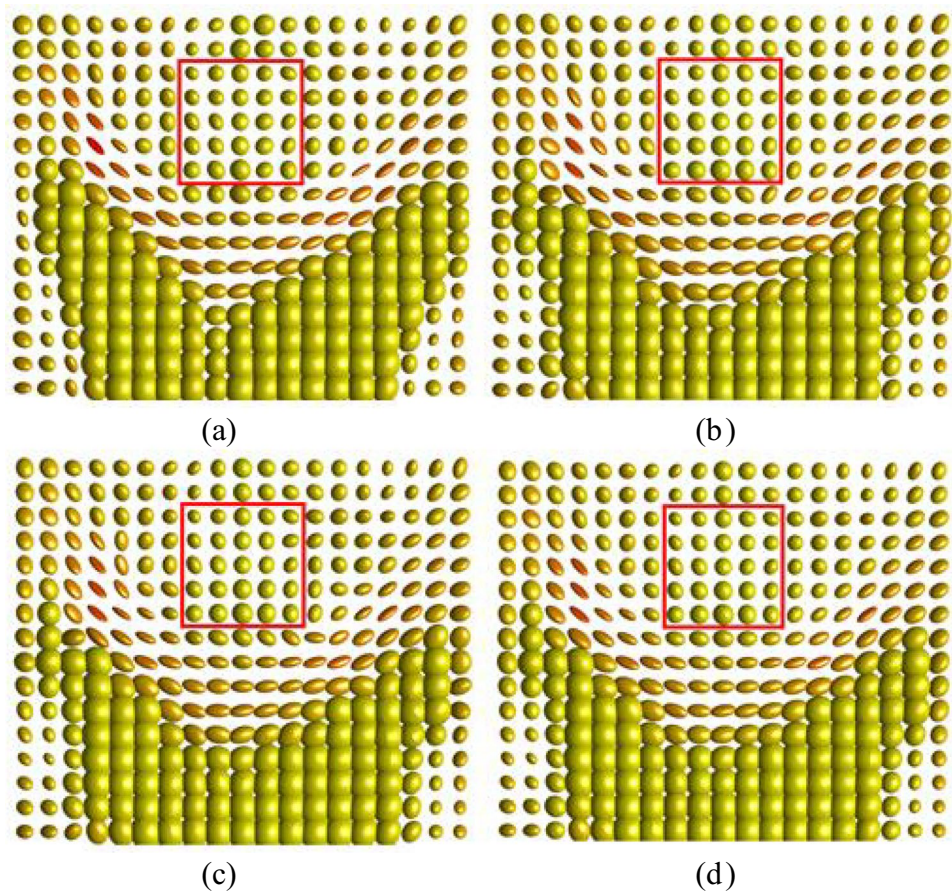
(a)          (b)

(c)          (d)

**Fig. 9** The contour of corpus callosum comparison. Top row: from left to right, the original tensor fields, SS interpolated results, SQ and Log-E interpolated results; bottom row: corresponding FA images of the original image, SS, SQ, and Log-E interpolated images
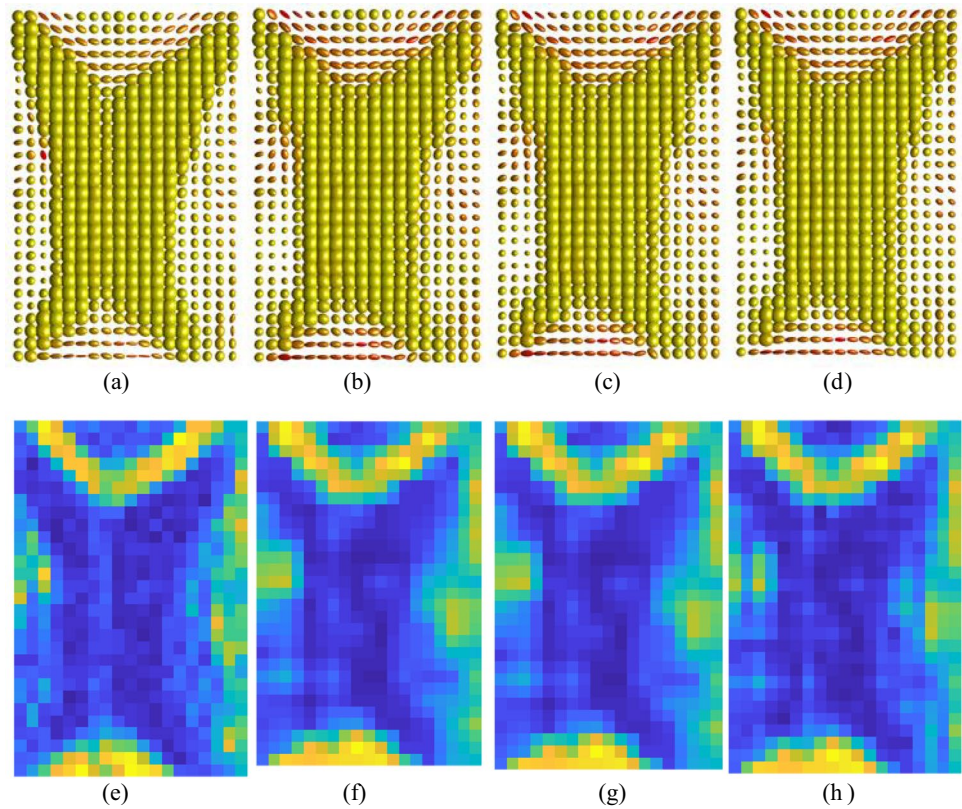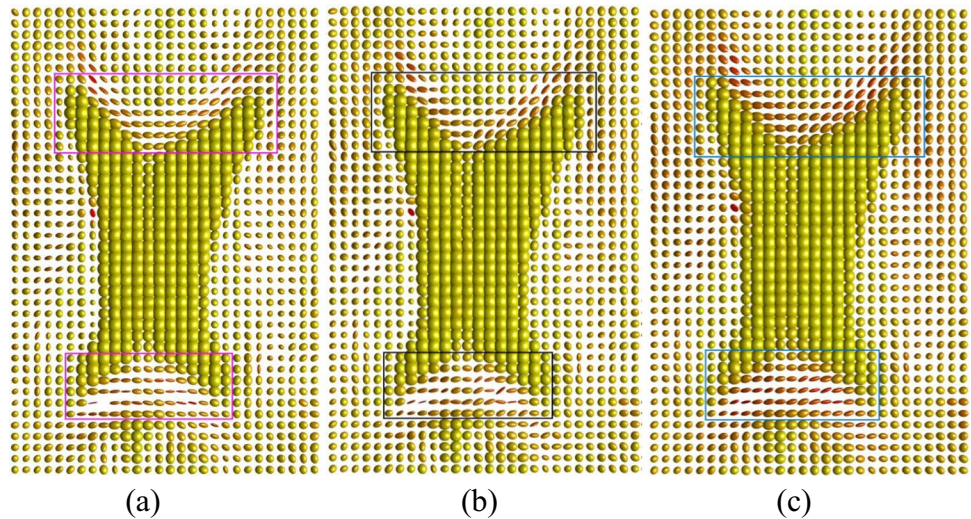


(a)      (b)      (c)      (d)

(e)      (f)      (g)      (h)

**Fig. 10** DTI Gaussian filtering experiment. **a** Original DTI brain data focusing corpus callosum; **b** noisy DTI data of image **a**; **c** Gaussian filtering result of image **b**



(a)      (b)      (c)

the brain corpus callosum, (b) is the noisy tensor display of (a), and (c) is the filtering result of (b). From the two black rectangle regions in figure (b), we can find that the shape and orientation of some tensors are askew, and the shape and orientation of tensors after filtering are improved significantly. At last, we give a brief algorithm steps for Gaussian filtering.

---

**Algorithm 1: DTI Gaussian Filtering**

**Inputs:** Local tensors $S_1, S_2, S_3, \ldots, S_N$ and Gaussian kernel coefficient $\omega_i$, $i = 1, \ldots, N$;

**Outputs**: The weighted tensor $S_{weighted}$ at the center of local region;

    1. Decompose $S_i = U_i \Lambda_i U_i^T$ with the eigenvalues in decreasing order;

    2. Preparing Gaussian filtering weighting template $\omega$;

    3. Compute DTI weighted mean eigenvectors matrix $U_{weighted}$ using equation (15):

$$U_{weighted} = \sum_{i=1}^{N} U_i \, diag(\frac{\sin \omega_i \theta_1}{\sin \theta_1}, \frac{\sin \omega_i \theta_2}{\sin \theta_2}, \frac{\sin \omega_i \theta_3}{\sin \theta_3});$$

    4. Compute DTI weighted mean eigenvalue matrix $\Lambda_{weighted} = \exp(\sum_{i=1}^{N} \omega_i \log \Lambda_i)$;

    5. Output the weighted tensor $S_{weighted} = U_{weighted} \Lambda_{weighted} U_{weighted}^T$.

---

## 5.2 DTI regularization

In the process of DTI acquisition, due to the influence of noise or some other factors, the shape and orientation of some diffusion tensors are usually blurred, which makes it difficult to identify the detailed edges or small lesions. In order to alleviate the influence of noise on the diffusion tensor image and to effectively preserve the edge or lesion information, regularization of DTI data is required. Due to the difficulty of dealing with DTI orientation information, the traditional scalar image regularization technique does not work for DTI images. Here we present a new DTI regularization procedure based on the SS framework on multidimensional interpolation. A brief step is listed as follows:

---

**Algorithm 2: DTI Regularization**

**Inputs:** Local neighbor tensors $S_1, S_2, S_3, \ldots, S_6$ around $S_0$, the weighting coefficients $\omega_i$, $i = 1, 2, \ldots, 7$;

**Outputs**: Regularized tensor $S_0'$ corresponding to $S_0$;

    1. Decompose $S_i = U_i \Lambda_i U_i^T$ with the eigenvalues in decreasing order;

    2. Construct the regularization weighting coefficients $\omega_i$;

    3. Compute the weighted mean eigenvectors matrix $U_{mean}$ using

$$U_{mean} = \sum_{i=1}^{7} U_i \, diag(\frac{\sin w_i \theta_1}{\sin \theta_1}, \frac{\sin w_i \theta_2}{\sin \theta_2}, \frac{\sin w_i \theta_3}{\sin \theta_3});$$

    4. Compute the weighted mean eigenvalue matrix $\Lambda_{mean} = \exp(\sum_{i=1}^{7} \omega_i \log \Lambda_i)$;

    5. Replace $S_0$ with the computed mean tensor $S_0' = U_{mean} \Lambda_{mean} U_{mean}^T$ pixel by pixel.

---

The regularization result of the above algorithm on real DTI data is reported in Fig. 11. In Fig. 11, (a) is the corpus callosum ROI in the central slice of brain DTI data, (b) is the zoom-in view of the pink rectangle region in figure (a), and figure (c) is the corresponding regularization ROI to figure

(b). It is clear after regularization, and the tensor's shape and orientation are normalized. The profile of tensors in the pink band of figure (b) and (c) is drawn in figure (d), where the Det, FA, HA, and IA indices profile are compared with different

**Fig. 11** Regularization results of a real brain DTI data. **a** Original tensor image of brain corpus callosum ROI; **b** zoom-in view of a in the pink rectangular; **c** regularization results of the corresponding region with **b**; **d** The Det, FA, HA, and IA curves corresponding to the tensors within the pink band in **b** and **c**
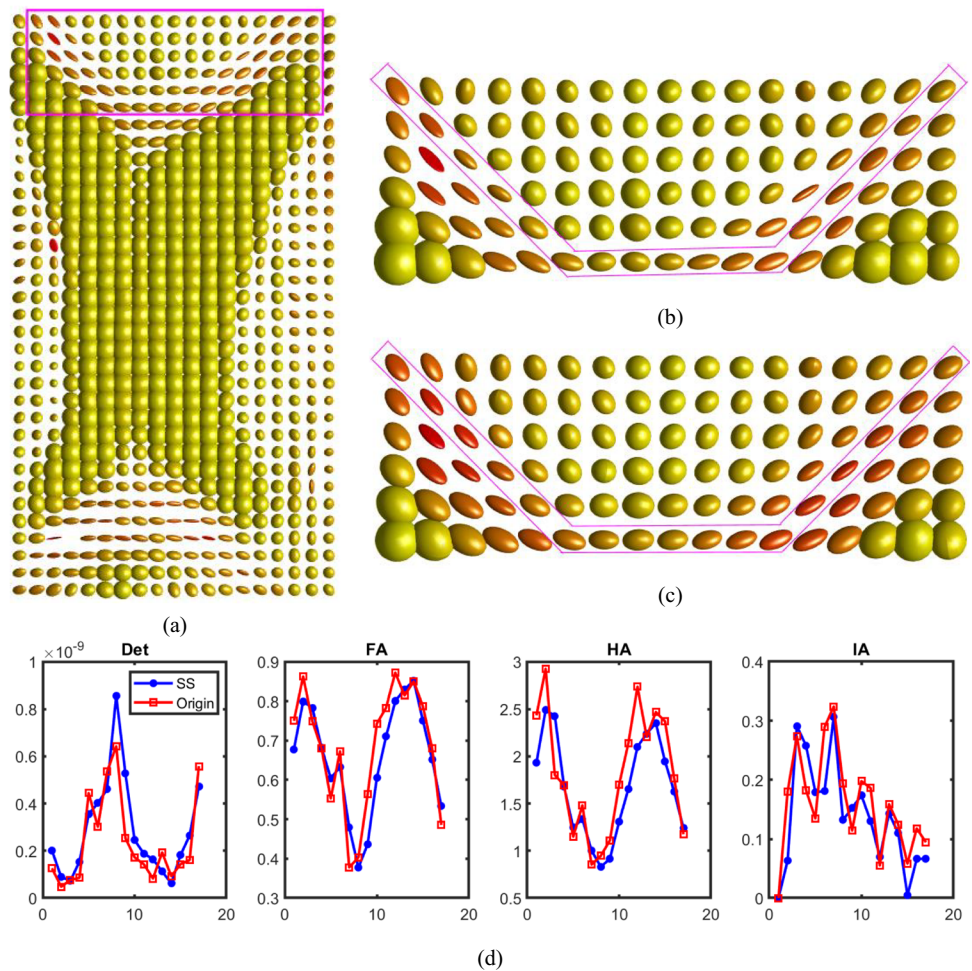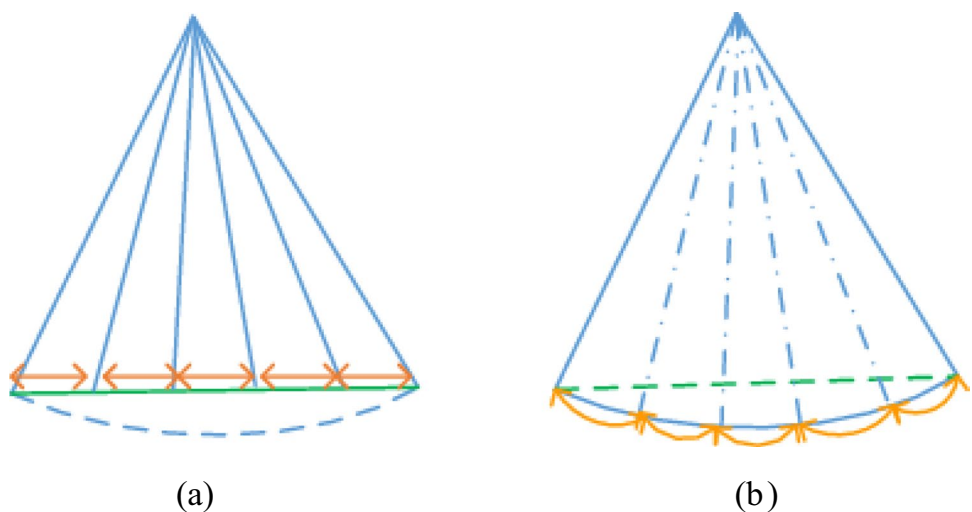


(a)

(b)

(c)

(d)

**Fig. 12** Demonstration of SQ and SS interpolation model. **a** SQ changes uniformly along the chord. **b** SS changes uniformly along the arc



(a)                                                                                       (b)

colors. The profiles after regularization are almost coincident with the original DTI data.

## 6 Discussion

This work proposed a new DTI interpolation framework named with spectrum-sine (SS) by connecting the spectrum of tensor to be interpolated with the spectrum of known tensors with some sine weights analytically. One-dimensional DTI interpolation strategy is built between two tensors in a geometric manner, in which the shape and orientation of interpolated tensors vary uniformly. As presented, a two-dimensional case is not a direct generalization of one-dimensional interpolation since the sum of four tensors is not twice of two. In a two-dimensional interpolation, the SS framework is further developed from the idea of geometric interpolation view. The orientation of the interpolated tensor should be included by the known four tensors. Based on this point, the two-dimensional interpolation strategy is successfully proposed. It should be pointed out, the try of twice of one-dimensional interpolation failed because the idea of bilinear is algebraic, not geometric in essence. For the multidimensional interpolation strategy, we can generalize the idea of the two-dimensional interpolation strategy. Another output accompanying the multidimensional interpolation method is the DTI mean definition under the SS framework. Thus far, the whole SS framework for DTI interpolation was proposed comprehensively.

The main merit of the SS interpolation framework is the tensor's orientation preservation. Most of the current DTI processing techniques try to transfer the tensor's high-dimensional information to one-dimensional scalar information; then, a lot of mature technique in scalar information processing can be used in DTI processing directly. In the DTI interpolation area, from element-wise linear interpolation to the Log-E framework, the tensor's high-dimensional information is approximated better and better, and until the SQ framework based on representing the tensor's orientation with quaternions ingeniously, the tensor's anisotropy feature was well preserved. As the SS framework is concerned, this is the first try to interpolate the tensor's orientation directly, and the good shape and rotation invariant property proposed in the SQ framework are all satisfied in SS. There is a small difference between SQ and SS framework, focusing on the orientation preservation; the interpolation of SQ is to make the changes vary uniformly along the chord direction while the SS framework is to lead the orientation changes to vary uniformly along the arc direction. This is further illustrated in Fig. 12, figure (a) is the demonstration of the SQ method, in which the length of each chord is equal, and figure (b) is for the SS method in which the length of each arc is equal. Therefore, the interpolated angles of SS are equal, and the angles of SQ are symmetric changing and near to equal.

Experiments were carried on both synthetic and real DTI data. In synthetic DTI data, the interpolation experiments between two tensors in 1D and four tensors in 2D were compared in detail with SS, SQ, and Log-E methods. The results show that the SS and SQ methods perform well in the preservation of the tensor's size, shape, anisotropy, and all scalar indices related to the eigenvalues. For the orientation of tensor, the interpolation results of two tensors and four tensors both show that the orientation variation obtained by the SS method is more homogeneous than SQ. In a real DTI data experiment, the three interpolation methods were further validated on brain images. No matter anisotropy and isotropy ROI, the interpolation performance of both SS and SQ is better than Log-E, and the difference between SS and SQ only lies in orientation variation. As the result of synthetic DTI data, the continuity of tensor's orientation in SS is a little better than SQ. For multidimensional interpolation and DTI mean methods validation, we further developed Gaussian filtering and regularization applications for DTI. The experimental result of DTI Gaussian filtering based on the SS framework shows that the procedure is satisfied on both the tensor's shape and orientation preservation. Regularization of DTI experimental results shows that the Det, FA, HA, and IA profile after regularization is coincident with the original DTI data, while the tensor's shape and orientation feature at some bad points were improved significantly. In addition, the computing complexity of the SS method is lower than that of SQ since there is no representation calculation process of quaternions or Euler angles of the spectrum.

Finally, we want to discuss the disadvantages of the current SS framework. For convenience, the whole method related to the SS framework in this work was deduced on positive diffusion tensors since no singular tensor is concerned. In theory, all of the tensors from DTI should be positive; however, there are some cases in real numerical implementation related to tensors close to singular. This is not covered by the current SS framework, which will be further supplemented in our future study.

## 7 Conclusion

In conclusion, a new spectrum-sine interpolation framework for DTI processing is proposed in this work. The SS framework for DTI processing was developed for two tensors interpolation, four tensors' interpolation, and multidimensional interpolation. Based on these interpolation methods, the idea of DTI mean was proposed using the multidimensional SS interpolation strategy. This is further developed for DTI Gaussian filtering and regularization. Experiments on synthetic and real brain DTI data both verify the effectiveness of the proposed DTI processing technique. In the near

future, we will apply the proposed SS interpolation framework in DTI registration for a better registration accuracy, especially on the principal direction accuracy, which is also important for DTI fiber tracking.

# References

1. Alexander DC, Pierpaoli C, Basser PJ, Gee JC (2001) Spatial transformations of diffusion tensor magnetic resonance images. IEEE Trans Med Imaging 20(11):1131–1139
2. Arsigny V, Fillard P, Pennec X, Ayache N (2006) Log-Euclidean metrics for fast and simple calculus on diffusion tensors. Magn Reson Med 56(2):411–421
3. Basser PJ, Pierpaoli C (1996) Microstructural and physiological features of tissues elucidated by quantitative-diffusion-tensor MRI. J Magn Reson 213(2):560–570
4. Batchelor PG, Moakher M, Atkinson D, Calamante F, Connelly A (2005) A rigorous framework for diffusion tensor calculus. Magn Reson Med 53(1):221–225
5. Bihan DL, Mangin JF, Poupon C, Clark CA, Pappata S, Molko N et al (2001) Diffusion tensor imaging: concepts and applications. Journal of magnetic resonance imaging : JMRI 13(4):534–546
6. Bro R, Acar E, Kolda TG (2008) Resolving the sign ambiguity in the singular value decomposition. J Chemom 22(2):135–140
7. Collard A, Bonnabel S, Phillips C, Sepulchre R (2014) Anisotropy preserving DTI processing. Int J Comput Vision 107(1):58–74
8. Fletcher PT, Joshi S (2007) Riemannian geometry for the statistical analysis of diffusion tensor data. Signal Process 87(2):250–262
9. Frindel C, Robini M, Schaerer J, Croisille P, Zhu YM (2010) A graph-based approach for automatic cardiac tractography. Magn Reson Med 64(4):1215–1229
10. Hoptman MJ, Nierenberg J, Bertisch HC, Catalano D, Ardekani BA, Branch CA et al (2008) A DTI study of white matter microstructure in individuals at high genetic risk for schizophrenia. Schizophr Res 106(2–3):115–124
11. Hui Z, Yushkevich PA, Alexander DC, Gee JC (2006) Deformable registration of diffusion tensor MR images with explicit orientation optimization. Med Image Comput Comput Assist Interv 8(1):172–179
12. Kindlmann G, Weinstein D, Hart D (2000) Strategies for direct volume rendering of diffusion tensor fields. IEEE Trans Visual Comput Graphics 6(2):124–138
13. Kindlmann, G., Raúl San José Estépar, Niethammer, M., Haker, S., & Westin, C. F. (2007). Geodesic-loxodromes for diffusion tensor interpolation and difference measurement. MICCAI pp. 1–9.
14. Moakher M (2005) A differential geometry approach to the geometric mean of symmetric positive-definite matrices. SIAM J Matrix Anal Appl 26(3):735–747
15. Peeters, T. H. J. M., Rodrigues, P. R., Vilanova, A., & Romeny, B. M. H. (2009). Analysis of distance/similarity measures for diffusion tensor imaging. Visualization and Processing of Tensor Fields. Springer Berlin Heidelberg.
16. Peng H, Orlichenko A, Dawe RJ, Agam G, Zhang S, Arfanakis K (2009) Development of a human brain diffusion tensor template. Neuroimage 46(4):967–980
17. Pennec X, Fillard P, Ayache N (2006) A Riemannian framework for tensor computing. Int J Comput Vision 66(1):41–66
18. Peter J, Basser M, J., & Denis LeBihan. (1994) MR diffusion tensor spectroscopy and imaging. Biophys J 66(1):259–267
19. Peyrat JM, Sermesant M, Pennec X, Delingette H (2007) A computational framework for the statistical analysis of cardiac diffusion tensors: application to a small database of canine hearts. IEEE Trans Med Imaging 26(11):1500–1514
20. Shoemake, K. (1985). Animating rotation with quaternion curves. Conference on Computer Graphics & Interactive Techniques. ACM, pp. 245–254.
21. Smith SM, Jenkinson M, Johansen-Berg H, Rueckert D, Nichols TE, Mackay CE et al (2006) Tract-based spatial statistics: voxelwise analysis of multi-subject diffusion data. Neuroimage 31(4):1487–1505
22. Son CI (2012) Diffusion tensor interpolation profile control using non-uniform motion on a Riemannian geodesic. Frontiers of Information Technology & Electronic Engineering 13(2):90–98
23. Toussaint, N; Sermesant, M; Stoeck, C T; Kozerke, & S; Batchelor. (2010). In vivo human 3D cardiac fibre architecture: reconstruction using curvilinear interpolation of diffusion tensor images. Med Image Comput Comput Assist Interv, pp. 418–425.
24. Wang Y, Chen Z, Nie S, Westin CF (2013) Diffusion tensor image registration using polynomial expansion. Phys Med Biol 58(17):6029–6046
25. Wang Z, Vemuri BC, Chen Y, Mareci T (2004) A constrained variational principle for direct estimation and smoothing of the diffusion tensor field from complex DWI. IEEE Trans Med Imaging 23(8):930–939
26. Weickert, J., & Welk, M. (2005). Tensor field interpolation with PDES.
27. Yang F, Zhu YM, Magnin IE, Luo JH, Croisille P, Kingsley PB (2012) Feature-based interpolation of diffusion tensor fields and application to human cardiac DT-MRI. Med Image Anal 16(2):459–481
28. Yu S, Ying L, Fuchun S (2012) Overview of tensor valued images interpolation technology. Journal of Image & Graphics 17(10):1197–1205
29. Zhukov, L., & Barr, A. H. (2002). Oriented tensor reconstruction: tracing neural pathways from diffusion tensor MRI. Visualization, pp. 387–394.

**Yuanjun Wang** , Associate Professor, received his BS and MS degree in Applied Mathematics and Ph.D. in Medical Informatics from Fudan University in June 2010. His research interest is medical image analysis and computer vision.

**Fan Jiang** , Ph.D. candidate, received her BS degree from the University of Shanghai for Science and Technology in June 2017. Her research interest is medical image processing.
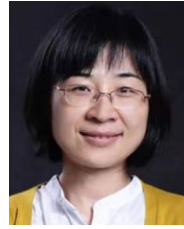


**Yu Liu** , M.D., radiologist in Shanghai Ninth People's Hospital, received her Ph.D. in Radiology Medicine at Shanghai Jiao Tong University School of Medicine. Her research interest is medical imaging.